applied sciences

MDPI

Article

Towards the Analytical Generalization of the Transcendental Energy Equation, Group Velocity, and Effective Mass in One-Dimensional Periodic Potential Wells with a Computational Application to Common Coupled Potentials

F. Mendoza-Villa [1], Erich V. Manrique-Castillo [1,*], Edson C. Passamani [2] and Juan A. Ramos-Guivar [1]

[1] Grupo de Investigación de Nanotecnología Aplicada para Biorremediación Ambiental, Energía, Biomedicina y Agricultura (NANOTECH), Facultad de Ciencias Físicas, Universidad Nacional Mayor de San Marcos, Av. Venezuela Cdra 34 S/N, Ciudad Universitaria, Lima 15081, Peru; freddy.mendoza1@unmsm.edu.pe (F.M.-V.); juan.ramos5@unmsm.edu.pe (J.A.R.-G.)
[2] Departamento de Física, Universidade Federal do Espírito Santo—UFES, Vitória 29075-910, ES, Brazil; passamaniec@yahoo.com.br
* Correspondence: emanriquec@unmsm.edu.pe

Featured Application: The findings presented in this work will allow the calculation of the electronic density states as well as the electrical and optical properties of complex one-dimensional coupled periodic potential wells without using expensive licensed software.

Abstract: The analytical generalization for N periodic potential wells coupled to a probe rectangular-like potential and a zero potential is extremely important in the study of one-dimensional periodic potentials in solid state physics, e.g., in the calculation of transport, optical, and magnetic properties. These findings raise the possibility of calculating equations for the generalization of N arbitrary potentials related to any potential $V(x)$ using special functions as a solution. In this work, a novel analytical generalization of the transcendental energy equation, group velocity, and effective mass for N-coupled potentials to a probe one-dimensional potential $V = V(x)$ was proposed. Initially, two well-known linear periodic potentials $V = V(x)$ were employed to obtain analytical solutions for rectangular-like and Dirac-delta potentials. Python libraries were used to easily represent the equations for one or two rectangular-like potentials coupled with an arbitrary potential, highlighting the transcendental energy, group velocity, and effective mass. The results showed that the group velocity behavior changed its orientation due to the sign of the potential, whereas the width of the potential $V(x)$ strongly influenced the group velocity behavior. The effective mass was also modified by the potential shapes, and their combinations, both effective mass and group velocity, exhibited similar physical behaviors to those found in ordinary rectangular-like potentials.

Keywords: Kronig–Penney model; Dirac-delta potential; periodic potentials; computational physics; rectangular-like potential; triangular-like potential; linear potential generalization of potentials

Citation: Mendoza-Villa, F.; Manrique-Castillo, E.V.; Passamani, E.C.; Ramos-Guivar, J.A. Towards the Analytical Generalization of the Transcendental Energy Equation, Group Velocity, and Effective Mass in One-Dimensional Periodic Potential Wells with a Computational Application to Common Coupled Potentials. *Appl. Sci.* **2024**, *14*, 3987. https://doi.org/10.3390/app14103987

Academic Editor: Mickaël Lallart

Received: 1 February 2024
Revised: 28 February 2024
Accepted: 28 February 2024
Published: 8 May 2024

1. Introduction

The inability of Newtonian physics to explain several phenomena on an atomic scale led scientists to search for new possibilities, and Quantum Mechanics (QM) was established at the beginning of the 20th century. The main result of QM is the Schrödinger equation (SE), which is equivalent to Newton's second law in classical mechanics [1]. One of the several phenomena that classical mechanics was not able to explain was the electrical conduction in solids, a phenomenon that QM was able to address using, for example, Kronig–Penney's periodic potential model [2,3].

Regarding this issue, there are several theoretical techniques to study the problem related to periodic potentials, such as the transfer matrix and theory of perturbations [4,5].

However, despite being effective methods, they also have some drawbacks. On the one hand, the transfer matrix method used to calculate physical properties using finite periodic potentials as the Dirac-delta is advantageous, while the theory of perturbations is successfully applied in Zeeman and Stark effects, e.g., [2,6–8]. On the other hand, it is important to note that both mentioned methods also have their intrinsic limitations. In the case of the transfer matrix, multiple matrix multiplications are required to obtain it, which can be computationally expensive [4,9]. In perturbation theory, one needs to simulate small variations in periodic potentials by using Bloch's theorem [10,11].

Besides the above issues, considering that the periodic potentials are basically barriers that repeat simulating regular intervals in a crystal lattice, without the use of Bloch's theorem, it would be necessary to solve multiple potentials, as described in Refs. [3,4], but a transcendental energy equation can be obtained using Bloch's theorem [9,12]. Thus, Bloch's theorem helps to simplify this type of calculation, as will be demonstrated by performing the generalization of N-coupled potentials to an arbitrary potential, i.e., by increasing the complexity of the problem, which may allow for a more realistic condition or some local perturbation that is not taken into account in an ordered periodic potential (e.g., to account for impurities that create different potentials and lengths in the chemical bounds).

On the one hand, periodic potentials, as previously mentioned, have a number of widely recognized applications in physics. For example, they are essential to explaining the electrical conduction of solids, which consequently leads to an understanding of the main differences between metals, semiconductors, and insulators [12–14]. In optical physics, they allow us to explain phenomena such as light reflection and explain why some solids have shine characteristics while others are opaque [14,15]. These observations are a direct consequence of band theory, which describes the electronic structure of solids and shows the existence of allowed and forbidden energy bands [2,12,14].

The tunneling effect is one of the main problems in solving symmetric or asymmetric potential barriers in QM [16]. For the simplest case (a rectangular-like barrier), the main goal is to determine the transmission and reflection coefficients through a potential barrier [17,18]. However, there are more complex barriers that involve combinations of potentials—for instance, a triangular-like potential coupled to a rectangular-like potential or a rectangular-like potential combined with a parabolic-like potential, i.e., potentials that approach a more realistic physical problems [19,20]. Again, Bloch's theorem can also be used to address the corresponding asymmetric-like potentials, which also reduces the computational costs.

In solid state physics, the Kronig–Penney model stands out as the simplest and most widely known periodic potential to explain band theory [3,12], unlike other potentials, such as linear-like or parabolic-like potentials [21–24]. It should be noted that the Kronig–Penney model has an analytical solution of time-independent SE, and the solutions are real exponential-like functions. On the other hand, other periodic potentials require the use of special functions, such as the Airy, Bessel, parabolic cylinder, or Mathieu functions [25–29]. Therefore, the solution of the secular determinant, applying the boundary and continuity conditions using Bloch's theorem, leads to the transcendental energy equation [3,12]. In addition, the question of how the group velocity and effective mass are obtained from this transcendental energy equation for coupled potentials together with a Dirac-delta potential is a problem that still needs further study.

In this work, a general solution to the transcendental energy equation (SE in k-space) for the rectangular-like barrier combined or not with other types of potential shapes was proposed. Under this condition, asymmetric $V = V(x)$ potentials were generated along with the rectangular-like potential. As a consequence, the transcendental energy equation, group velocity, and effective mass were obtained for a periodic potential in the form of a rectangular barrier combined with any $V = V(x)$ potential. Moreover, the generalization of the energy equation, group velocity, and effective mass for N-coupled potentials along with a zero-like or rectangular-like potential was calculated, this research being more general than that described in Ref. [30].

2. Theoretical Model Background and Simulation Details

The potential $V = V(x)$ is a function of height w and is coupled to a rectangular-like barrier of height w_0. However, the following condition is required: the potential $V = V(x)$ must approach zero potential when the height of the potential barrier w tends to zero.

$$\lim_{w \to 0} (V(w)) = 0 \tag{1}$$

Figure 1 represents the approximation of the Kronig–Penney model, the potential to which the other potentials studied will be approximated, and those that meet the condition of Equation (1).

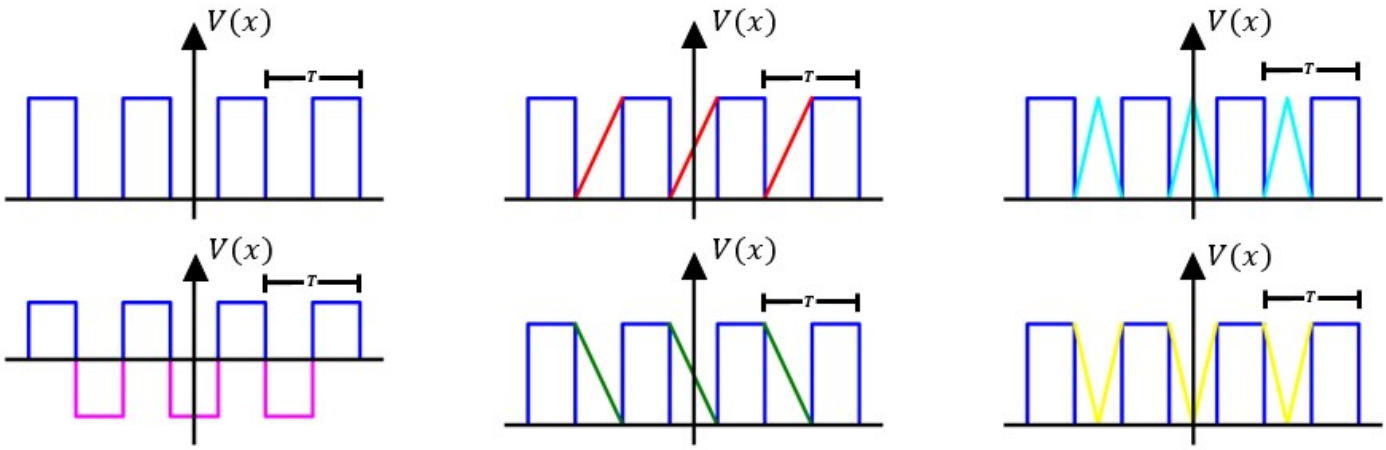

Figure 1. Schemes of the quantum potentials. The dark blue lines represent the Kronig–Penney potential. The are due to the rectangular-like potential of negative intensity (magenta color). The red and green lines represent the linear-like potentials, while the cyan and yellow lines are the triangular-like potentials.

The solutions of the potentials displayed in Figure 1 of the associated time-independent SE are commonly special functions [22,23,26,31], while the zero-like potential has its solution as a linear combination of complex exponentials [3].

To treat these periodic potentials, the same method proposed for potentials approximating the Dirac-delta potential was used [12,14], but with the assumption that the potential $V = V(x)$ must now satisfy Equation (1). For this, the well-known Bloch theorem, widely used in periodic potentials, was applied [32]. In other words, a is the width of the rectangular-like potential, $2b$ is the width of the potential $V = V(x)$, and $T = 2b + a$ is the period of the periodic potential (see Figure S1), while $\Psi_I(x)$, $\Psi_{II}(x)$, and $\Psi_0(x)$ represent the wave functions and $\Psi'_I(x)$, $\Psi'_{II}(x)$, and $\Psi'_0(x)$ are the derivatives of the wave functions. The applied contour and continuity functions have the same form as in [30]. Furthermore, the application of these is shown in the Supplementary Materials.

It has been reported in the literature [3,9,11,12] that Equations (2) and (3) have solutions for the cases of the rectangular-like potential and the Dirac-delta potential of positive intensity given, respectively, by

$$\cos(k(a+2b)) = \left(\frac{\beta^2 - \alpha^2}{2\beta\alpha}\right) \sinh(2b\beta) \sin(\alpha a) + \cosh(2b\beta) \cos(\alpha a) \tag{2}$$

$$\cos(ka) = \frac{P}{\alpha a} \sin(\alpha a) + \cos(\alpha a) \tag{3}$$

Equation (2) tends to Equation (3), resulting in an infinitely thin barrier width and an infinitely long potential barrier height. In Equations (2) and (3), the a and b parameters are defined in Figure 1. P is a positive intensity of the Dirac-delta potential, and the parameters that define the energies are $\alpha = \sqrt{2mE}/\hbar$ and $\beta = \sqrt{2m(w_0 - E)}/\hbar$. Then,

in Figure S1, the numerical simulation of the Kronig–Penney potential energy is plotted, starting from the analytical solution of Equation (2). For the simulations in the figures below, an approximation $\hbar^2/2m = 1$ is made in order to reduce the number of physical constants of the problem (it can be easily recovered at the end if necessary using this transformation and comparing the dimensions of the physical quantities [10]). In other words, this approximation does not affect the physics of the simulations. However, with this approximation, it is not necessary to place units in the simulations.

In Equation (2), $k = 1/\lambda$, where λ is the wavelength of the electrons. This is also important because the wave vector is usually defined as $k = 2\pi/\lambda$, which takes discrete values from $-\pi/T$ to π/T and thus defines the Brillouin zone. In this case, the trigonometric functions in Equations (4)–(7) are periodic with period $k.T$. It is worth mentioning that the units of k are the opposite of those of the period T. However, again, for simulation facilities, the transcendental energy $E(k)$ was plotted against the $k.T$ product.

The equations for the transcendental equation of energy, group velocity, and effective mass for an arbitrary potential $V(x)$ together with a rectangular-like potential are demonstrated in detail in Sections S1–S5 of the Supplementary Materials, following the next equations:

$$\cos(k(2b+a)) = \frac{\sinh(\beta a)}{\beta}\left[\frac{M_1(E) - \beta^2 M_2(E)}{M_4(E)}\right] + \cosh(\beta a)\left[\frac{M_3(E)}{M_4(E)}\right] \quad (4)$$

$$\cos(k(2b+a)) = \frac{\sinh(\beta a)}{\beta}\left[\frac{N_1(E) - \beta^2 N_2(E)}{N_4(E)}\right] + \cosh(\beta a)\left[\frac{N_3(E)}{N_4(E)}\right] \quad (5)$$

$$v_G = -\frac{T\sin(kT)}{\hbar H_0(E)} \quad (6)$$

$$m^* = \frac{-\hbar^2 H_2(E)}{T^2\cos(kT) + \hbar^2 v_G^2 H_1(E)} \quad (7)$$

Numerical simulations of the energy, group velocity, and effective mass were performed using the Numpy and Simpy libraries of the Python programming language version 3.7.9. The results obtained from the simulation were plotted in the OriginPro 9.0 software.

3. Results

3.1. Periodic Potential of One Potential $V = V(x)$ and a Rectangular-like Barrier

3.1.1. Rectangular-like Potential of Negative Intensity

The energy functions $M_1(E)$, $M_2(E)$, $M_3(E)$, and $M_4(E)$ for rectangular-like potentials of negative intensity are given by Equations (8)–(12):

$$M_1(E) = 2i\alpha_r^2 \sin(2\alpha_r b) \quad (8)$$

$$M_2(E) = 2i\sin(2\alpha_r b) \quad (9)$$

$$M_3(E) = -4i\alpha_r \cos(2\alpha_r b) \quad (10)$$

$$M_4(E) = -4i\alpha_r \quad (11)$$

where

$$\alpha_r = \frac{\sqrt{2m(w+E)}}{\hbar} \quad (12)$$

Figure 2 displays the energy dispersion and transcendental energy distribution for the rectangular-like potential with negative intensity calculated using Equations (8)–(12). The results align with those found in a rectangular-like potential equation when w tends to zero, i.e., it is $\cos(k(a+2b)) = \left((\beta^2 - \alpha_r^2)/(2\beta\alpha_r)\right)\sinh(a\beta)\sin(2\alpha_r b) + \cosh(a\beta)\cos(2\alpha_r b)$.

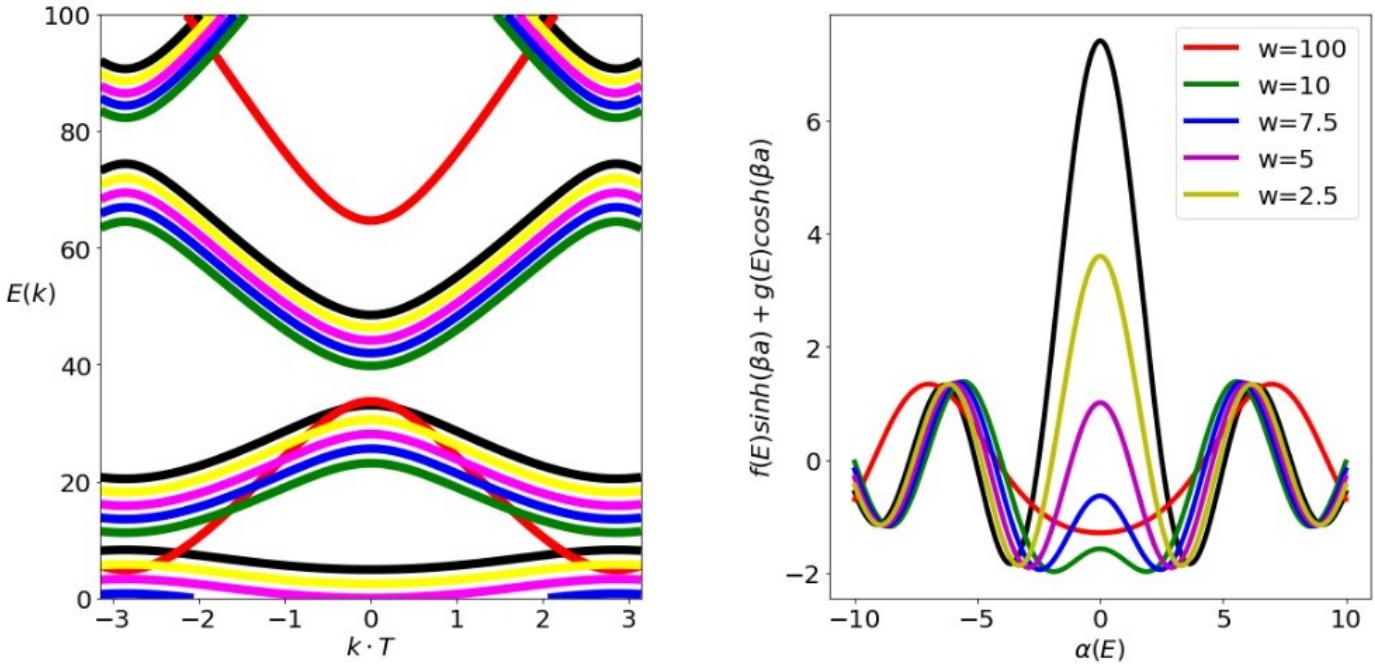

Figure 2. Left-hand side: Energy dispersion relation obtained from a rectangular-like periodic potential of negative intensity. Right-hand side: Transcendental energy equation as a function of energy parameter $\alpha = \sqrt{2mE}/\hbar$ simulated for different values of w (barrier height). The parameters were $w_0 = 100$, $a = 1/10$, and $b = 1/2$. Black curves are results from a pure rectangular-like potential with a positive intensity.

The energy curves are similar to those shown in Figure 2 for a pure rectangular-like potential. There is a difference in their behaviors for different w-values. For instance, at $w = 100$, the behavior differs from that of cases with distinct w-values. The amplitude and concavity of the energy distribution close to $\alpha = 0$ also vary.

3.1.2. Linear Potential with a Positive Slope

The energy functions $M_1(E), M_2(E), M_3(E)$, and $M_4(E)$ obtained for a linear-like potential with a positive slope are given by Equations (13)–(17):

$$M_1(E) = Ai^{'}(u_1(b))Bi^{'}(u_1(-b)) - Ai^{'}(u_1(-b))Bi^{'}(u_1(b)) \quad (13)$$

$$M_2(E) = Bi(u_1(-b))Ai(u_1(b)) - Bi(u_1(b))Ai(u_1(-b)) \quad (14)$$

$$M_3(E) = Ai(u_1(b))Bi^{'}(u_1(-b)) - Ai^{'}(u_1(-b))Bi(u_1(b)) + Ai(u_1(-b))Bi^{'}(u_1(b)) - Ai^{'}(u_1(b))Bi(u_1(-b)) \quad (15)$$

$$M_4(E) = 2W\{y_1(x), z_1(x)\} \quad (16)$$

where

$$u_1(x) = \left(\frac{2\sqrt{2m}b}{w\hbar}\right)^{2/3}\left(\frac{w}{2b}x + \frac{w}{2} - E\right) \quad (17)$$

Figure 3 shows the energy dispersion and transcendental energy distribution for the linear-like potential with positive intensity calculated using Equations (13)–(17).

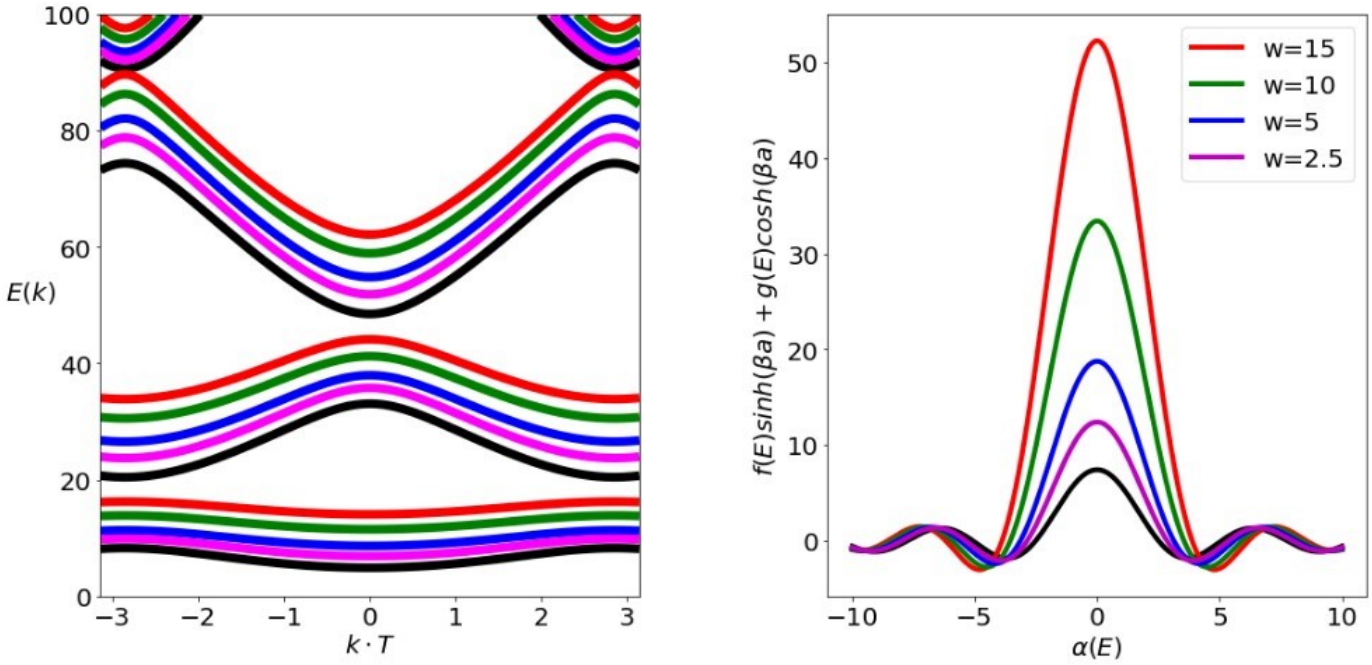

Figure 3. Left-hand side: Energy dispersion relation obtained from a linear periodic potential of positive slope. Right-hand side: Behavior of the transcendental energy equation as a function of the simulated alpha energy parameter for different values of w. The parameters were $w_0 = 100$, $a = 1/10$, and $b = 1/2$. Results for pure rectangular-like potential are also added in the plots, as shown by black curves.

3.1.3. Linear Potential with a Negative Slope

The energy functions $M_1(E), M_2(E), M_3(E)$, and $M_4(E)$ obtained for a linear-like potential with a negative slope are given by Equations (18)–(22):

$$M_1(E) = Ai^{'}(u_2(b))Bi^{'}(u_2(-b)) - Ai^{'}(u_2(-b))Bi^{'}(u_2(b)) \quad (18)$$

$$M_2(E) = Bi(u_2(-b))Ai(u_2(b)) - Bi(u_2(b))Ai(u_2(-b)) \quad (19)$$

$$M_3(E) = Ai(u_2(b))Bi^{'}(u_2(-b)) - Ai^{'}(u_2(-b))Bi(u_2(b)) + Ai(u_2(-b))Bi^{'}(u_2(b)) - Ai^{'}(u_2(b))Bi(u_2(-b)) \quad (20)$$

$$M_4(E) = 2W\{y_1(x), z_1(x)\} \quad (21)$$

where

$$u_2(x) = \left(\frac{-2\sqrt{2m}b}{w\hbar}\right)^{2/3}\left(-\frac{w}{2b}x + \frac{w}{2} - E\right) \quad (22)$$

Figure 4 shows the energy dispersion and transcendental energy distribution for the linear-like potential with negative intensity calculated using Equations (18)–(22).

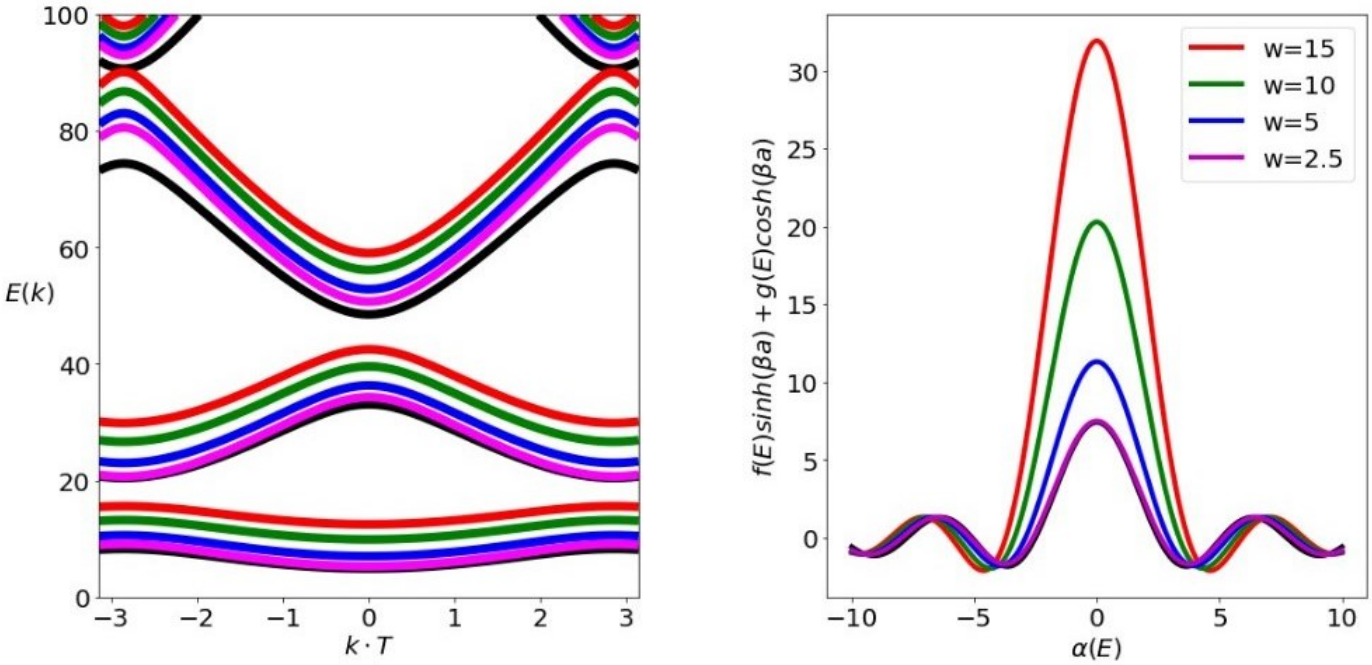

Figure 4. Numerical simulation of the transcendental energy equation for the negative-sloping linear periodic potential together with the rectangular potential at different values of w. The parameters were $w_0 = 100$, a = 1/10, b = 1/2. Results for pure rectangular-like potential are also added in the plots, as shown by black lines.

3.2. Group Velocity and Effective Mass for Rectangular-like Potentials of Negative Intensities

An important result from this analysis of periodic potentials is the fact that, depending on the height value of the rectangle of negative intensity, the group velocity can have its direction changed, as can be observed by comparing the results shown in Figure 5A,B. This behavior of the group velocity is due to the relation of $\alpha_r(E)$ in Equation (12). On the other hand, it should be mentioned that this factor is the only parameter that differentiates a rectangular-like potential with negative intensity from the transcendental equation of potential energy of Kronig–Penney. In other words, the relation of $\alpha_r(E)$ of Equation (12) is different from that of $\alpha(E) = \sqrt{2mE}/\hbar$, where the latter does not depend on the w-value. Therefore, the dependence of the parameter on w inevitably alters the behavior of the group velocity and effective mass, as shown in Figure 5A,B. More specifically, Figure 5A,C represent the group velocity and effective mass for heights of $w = 100$ (green color) and $w = 10$ (red color), while Figure 5B,D represent the group velocity and effective mass for heights of $w = 125$ (green color) and $w = 25$ (red color).

Figure 6 shows the transcendental energy equation as a function of energy for different heights w of rectangular potential: red for $w = 10$ and blue for $w = 100$. Thus, this figure clearly explains why the group velocity changes orientation, i.e., as $\cos(kT)$ must always be equal to ± 1. Figure 6 displays the different energy positions where there is an intersection of the energy function to satisfy the condition $\cos(kT) = f(E)\sinh(\beta a) + g(E)\cosh(\beta a)$. This effect occurs because of the value of $\alpha_r(E)$, which is dependent on the w-value.

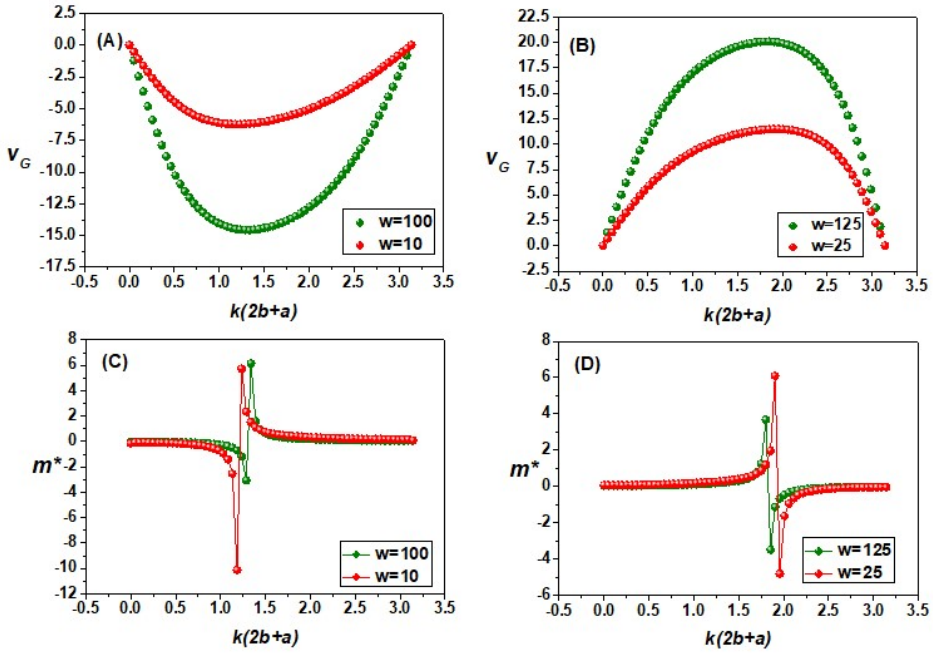

Figure 5. Numerical simulation of the group velocity (**A**,**B**) and effective mass (**C**,**D**) for the rectangular-like potential for a negative intensity. The curves were obtained for 62 different energy values. The parameters were $w_0 = 100$, $a = 1/10$, and $b = 1/2$.

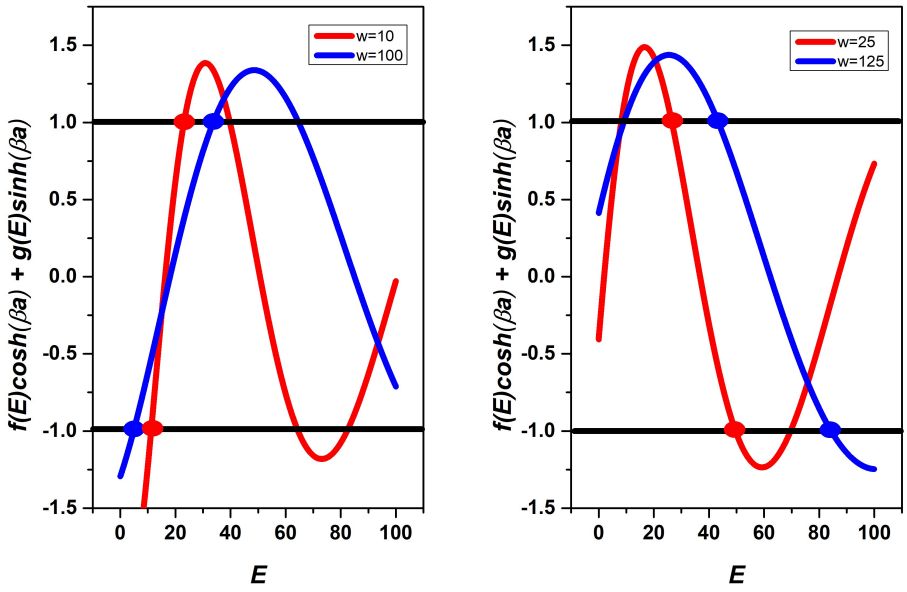

Figure 6. Behaviors of the numerical transcendental energy equation as a function of the energy for four different heights (w-values). The horizontal lines represent maximum limits for the $\cos(kT)$. The parameters were $w_0 = 100$, $a = 1/10$, and $b = 1/2$.

Group Velocity and Effective Mass for Linear Potentials

Figure 7 shows the behaviors of the group velocity (Figure 7A,B) and effective mass (Figure 7C,D) for high w-values: $w = 125$ (blue curve), $w = 50$ (green curve), $w = 10$ (magenta curve), and $w = 1$ (red curve). These two physical quantities were numerically simulated using two slopes for the linear-like periodic potential: a positive slope in Figure 7A,C and a negative slope in Figure 7B,D.

In contrast, Figure 8 displays the behaviors of the group velocity (Figure 8A,B) and effective mass (Figure 8C,D) numerically calculated for low w-values: $w = 0.001$ (blue

curve), $w = 0.01$ (green curve), $w = 0.1$ (magenta curve), and $w = 1$ (red curve). Again, the two physical quantities were numerically simulated using two slopes for the linear-like periodic potential: a positive slope in Figure 8A,C and a negative slope in Figure 8B,D.

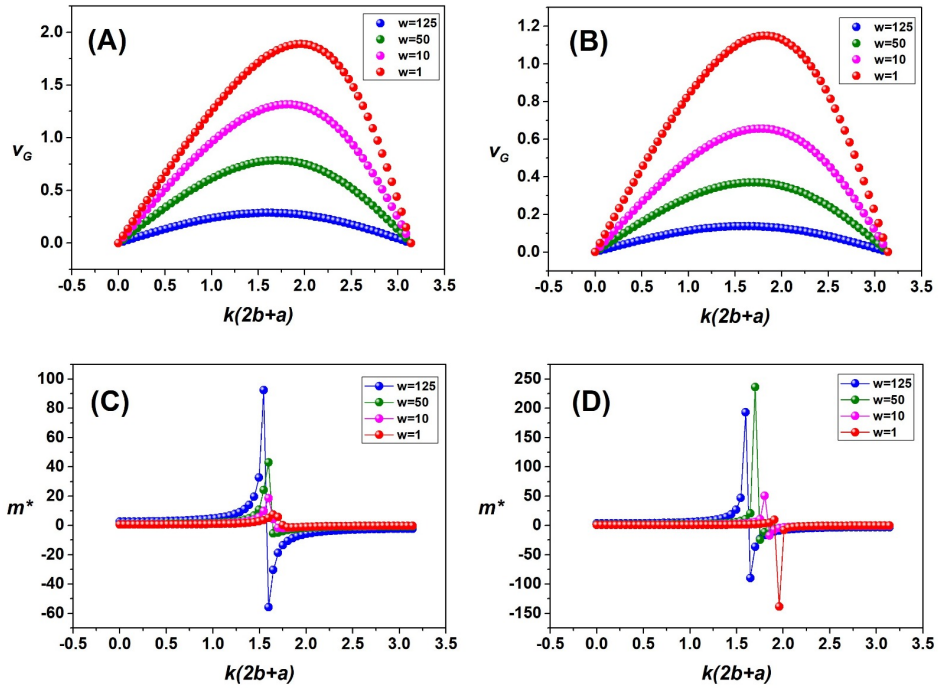

Figure 7. Numerical simulation of the group velocity (**A**,**B**) and effective mass (**C**,**D**) for two slopes of the linear–linear potential: positive slope in (**A**,**C**) and negative slope in (**B**,**D**). The curves were obtained for 62 different energy values and with high w-values. The parameters were $w_0 = 100$, $a = 1/10$, and $b = 1/2$.

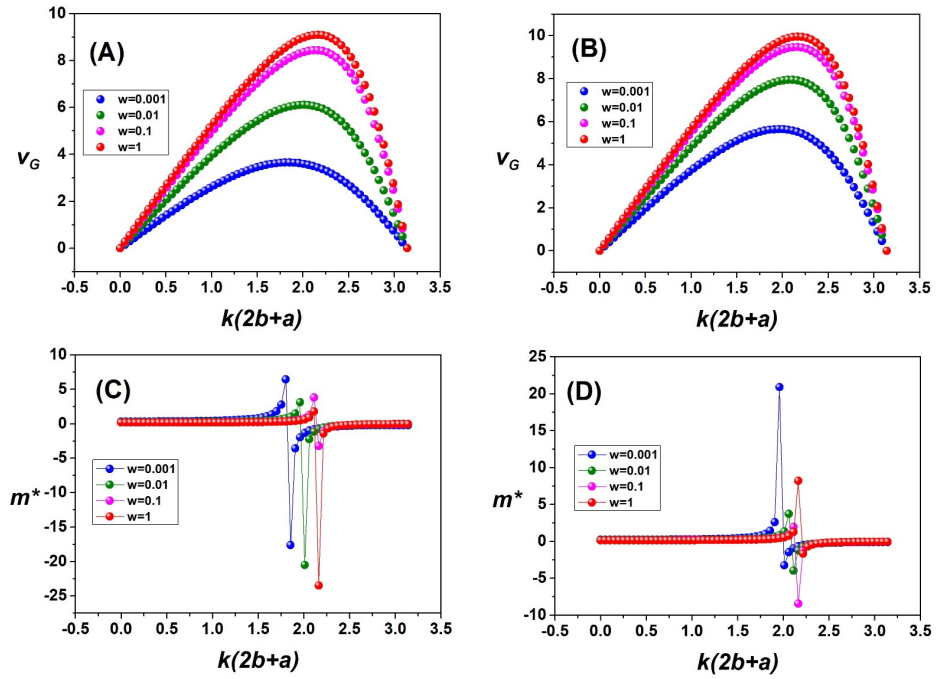

Figure 8. Numerical simulation of the group velocity (**A**,**B**) and effective mass (**C**,**D**) for two slopes of the linear–linear potential: positive slope in (**A**,**C**) and negative slope in (**B**,**D**). The curves were obtained for 62 different energy values and with low w-values. The parameters were $w_0 = 100$, $a = 1/10$, and $b = 1/2$.

4. Discussion

From the periodic potentials here proposed, it has been possible to corroborate the hypothesis that they can approach the Kronig–Penney model, i.e., the rectangular-like potential with a negative intensity and linear-like potentials can also yield results similar to those found in the Kronig–Penney model. For triangular-like potentials, a divergence in numerical calculation occurred, avoiding additional testing, as shown in Figures S2 and S3. In Figure 5, it can be seen that the orientation of the group velocity in the first band energy changes for certain values of w (potential height), i.e., either for values less than or greater than $w_0 = 100$. This may be explained considering that the rectangle at the interval $[-b, b]$ is of negative intensity. However, its energy dispersion is close to that found for the Kronig–Penney model, as can be seen in Figure 2.

The energy $H_0(E)$ function in Figure S4 expresses the variation in the group velocity in the rectangular-like potential of negative intensity, in agreement with the results shown in Figure 6. Therefore, the results in Figure S4 demonstrate that the orientation of the group velocity depends on which value of $\cos(kT) = \pm 1$ is crossed first. Thus, if the rate of change is positive, then the group velocity is positive, and vice versa [33]. In addition, two general issues can be stated: (i) the change in the sign of the group velocity has been evidenced in the numerical simulation of the second energy band when performed at potentials $V = V(x)$ that are close to a Dirac-delta potential, and (ii) the change in the orientation of the group velocity is not a particular case.

Table 1 shows the orientation changes in the group velocity when varying each of the parameters of the periodic rectangular-like potential of negative intensity.

Table 1. Group velocity for rectangular-like potential of negative intensity.

First Energy Band	w_0	a	w	b
v_G positive	100	1/10	125	1/2
	100	1/10	25	1/2
	75	1/10	5	1/3
	75	1/10	5/2	1/3
	50	1/5	25	1/2
	50	1/5	150	1/2
	150	1/10	30	1/2
	150	1/10	150	1/2
	150	1/5	100	1/3
	150	1/5	120	1/3
V_G negative	100	1/10	100	1/2
	100	1/10	10	1/2
	75	1/10	10	1/3
	75	1/10	25	1/3
	50	1/5	10	1/2
	50	1/5	100	1/2
	150	1/10	20	1/2
	150	1/10	100	1/2
	150	1/5	20	1/3
	150	1/5	30	1/3

Cases in which the group velocity changes its orientation in the first energy band for the rectangular-like potential of negative intensity.

The linear-like potentials also approximate the Kronig–Penney potential, as shown in Figures 3 and 4. However, on the right-hand side of these figures, it is observed that the potential rapidly approaches the one with a negative slope. For the group velocity using linear-like potentials, a peculiarity occurs in comparison with the results of the rectangular-like potential with negative intensity. For linear-like potentials, the numerically calculated group velocities for low and high values of w first show an increase in their group velocity until it reaches a maximum, whereby it subsequently decays for higher values of k, as

shown in Figures 7 and 8. In other words, the group velocity curves show an asymmetric parabolic-like behavior, with their maxima slightly depending on the w-value.

One possible explanation for the group velocity behaviors shown in Figures 7 and 8 is related to the width of the linear-like potential being smaller than that of the rectangular-like potential of positive intensity, i.e., $a = 1/10$ and $b = 1/2$, since, when the simulation of the Kronig–Penney model is done for parameters in which $b > a$, a trend in group velocity observed in Figures 7 and 8 is found. Figure 9 displays the group velocities and effective masses for $w_0 = 100$, $a = 1$, and $b = 1/3$ for a linear-like potential with two slopes: negative (Figure 9A,B) and positive (Figure 9C,D). This figure suggests that the relationship between the parameters a and b determines the behavior of the group velocity. When $a < b$, it has the behavior shown in Figures 7 and 8, while, when $b < a$, the behavior is presented as in Figure 9 [33–35]. Here, it should be stated that the Airy functions are not responsible for the observed divergence in the results because the used values are neither too small nor too large to provoke an appreciable divergence in the Airy functions. The Airy functions cannot be completely ruled out because they are improper integrals and cannot be expressed in terms of elementary functions; in other words, they are special functions [25,36].

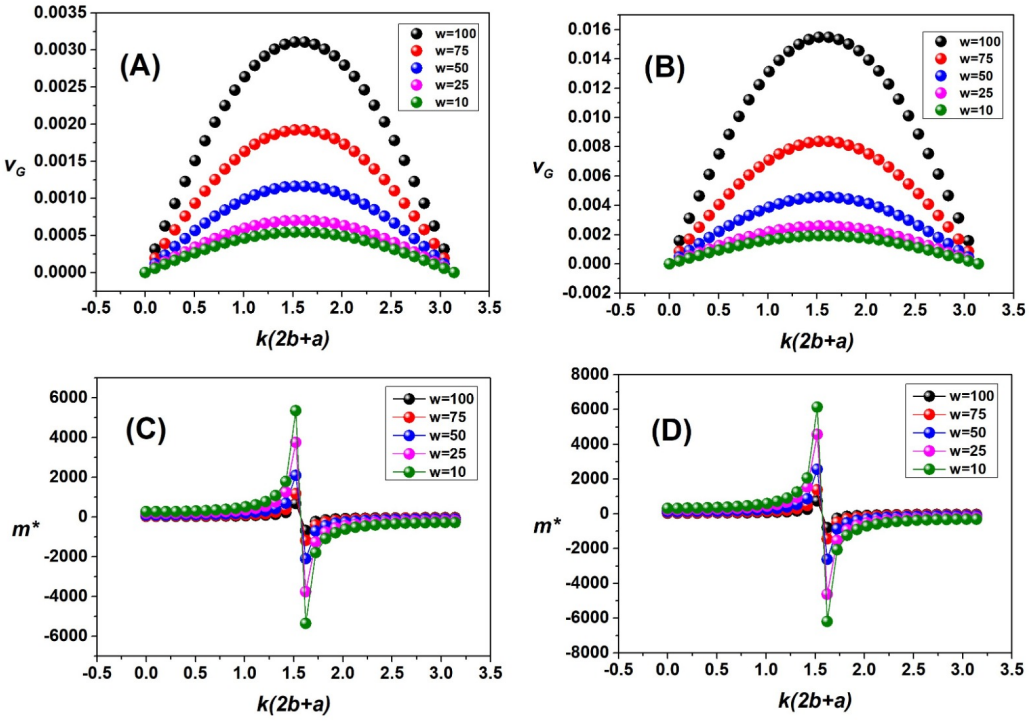

Figure 9. Numerical simulation with the values of $w_0 = 100$, $a = 1$, $b = 1/3$ for the group velocity (**A**,**B**) and the effective mass (**C**,**D**) for the linear-like potential. The data were obtained for 32 energy values. (**A**,**C**) show data obtained for positive-sloping linear-like potential and (**B**,**D**) show data obtained for negative-sloping linear-like potential.

The width of the rectangle also plays an important role in the results of the linear-like potential, mainly regarding whether it slopes positively or negatively, as mentioned in the previous paragraphs. The reason behind this is that if the width of the rectangle is much smaller than the width of the line and the height of the rectangle is constant, then a pseudo-Dirac-delta potential would be simulated. This behavior was visualized when the simulations of the Dirac-delta potential were made, as shown in Figure S1. However, there is a major difference: the width is not infinitely small, and the height is not infinitely high.

Table 2 shows the comparison of the positive and negative group velocities between the linear potentials. It is evident that the maximum of the group rate of the negative-

sloping linear-like potential decays faster than the maximum of the group rate of the positive-sloping linear-like potential.

Table 2. Group velocity for linear potentials with two slopes: positive and negative.

Group Velocity	w	kT	v_G
Positive slope linear potential	100	1.62	0.01550
	75	1.62	0.00835
	50	1.62	0.00456
	25	1.62	0.00257
	10	1.62	0.00192
Negative slope linear potential	100	1.62	0.003110
	75	1.62	0.001920
	50	1.62	0.001160
	25	1.62	0.000701
	10	1.62	0.000544

Comparison of group velocity between linear potentials. The parameters were $w_0 = 100$, $a = 1$, and $b = 1/3$.

Table 3 shows the comparison of the effective mass for the positive and negative linear-like potentials. The same is evident for the discontinuity energy; the negatively sloped linear-like potential decays faster than the positively sloped linear potential.

Table 3. Effective mass for linear potentials with two slopes: positive and negative.

Effective Mass	w	kT	E
Positive slope linear potential	100	1.57	62.2
	75	1.57	52.5
	50	1.57	41.9
	25	1.57	30.2
	10	1.58	22.1
Negative slope linear potential	100	1.57	59.4
	75	1.57	49.9
	50	1.57	39.3
	25	1.57	27.6
	10	1.57	19.3

Comparison of effective mass between linear potentials. The parameters were $w_0 = 100$, $a = 1$, and $b = 1/3$.

In the case of triangular-like potentials, their group velocities and effective masses cannot be simulated correctly due to the divergence shown in Figures S2 and S3. Moreover, for the triangular and inverted triangular-like potential, the divergence in the transcendental energy equation is clearly observed. This divergence is the product of the Airy functions, which are defined by improper integrals and simulated numerically [37]. Now, a generalization for the periodic potential with any shape can be proposed, i.e., the generalization that can be developed for the rectangular-like potential by considering arbitrary N potentials of the form $V = V(x)$ coupled in an interval $[-b, b]$. It should be noted that, interestingly, it has the same forms given in Equations (4) and (5) as can be seen in Equation (23).

$$\cos(kT) = \sinh(\beta a)\left[\frac{H_1^2(E) - \beta^2 H_4^2(E)}{2\beta H_0^0(E)}\right] + \cosh(\beta a)\left[\frac{H_2^2(E) - H_4^1(E)}{2H_0^0(E)}\right] \tag{23}$$

In turn, it can also be generalized for the zero-like potential coupled to arbitrary N potentials of the form $V = V(x)$, as shown in Equation (24).

$$\cos(kT) = \sin(\alpha a)\left[\frac{H_1^2(E) + \alpha^2 H_4^2(E)}{2\alpha H_0^0(E)}\right] + \cos(\alpha a)\left[\frac{H_2^2(E) - H_4^1(E)}{2H_0^0(E)}\right] \tag{24}$$

An interesting point about Equations (23) and (24) is that they have a similar form to Equations (2) and (3) for particular cases and to the equations of the transcendental energy equation when approximating to the Dirac-delta potential [30]. The elements of the matrix $H(E)$ shown in Equations (23) and (24) represent energy determinants, which are the result of Bloch's theorem for N + 1 potentials, being a rectangular-like potential or, alternatively, a zero-like potential. The equation of the matrix $H(E)$ is given by Equation (25).

$$H(E) = \begin{bmatrix} H_1^1(E) & H_1^2(E) & H_1^3(E) \\ H_2^1(E) & H_2^2(E) & H_2^3(E) \\ H_3^1(E) & H_3^2(E) & H_3^3(E) \\ H_4^1(E) & H_4^2(E) & H_4^3(E) \end{bmatrix} \tag{25}$$

With the obtained results, a generalized theorem can be proposed for periodic potentials having the studied form; see Appendices A and B. This theorem is of great importance because it helps to simplify the mathematical calculations of arbitrary N-coupled potentials to a potential with known wave functions. Equations (26) and (27) provide this energy function.

$$\Gamma(E) = -\Lambda(E) \tag{26}$$

$$\begin{aligned} \Gamma(E) = & \frac{H_4^2(E)}{2H_0^0(E)W\{y_{n+1}, z_{n+1}\}}\left[z'_{n+1}(b_{n+1})y'_{n+1}(b_m) - z'_{n+1}(b_m)y'_{n+1}(b_{n+1})\right] \\ & + \frac{H_1^2(E)}{2H_0^0(E)W\{y_{n+1}, z_{n+1}\}}\left[z_{n+1}(b_{n+1})y_{n+1}(b_m) - z_{n+1}(b_m)y_{n+1}(b_{n+1})\right] \\ & + \frac{H_2^2(E)}{2H_0^0(E)W\{y_{n+1}, z_{n+1}\}}\left[-z'_{n+1}(b_{n+1})y_{n+1}(b_m) + z_{n+1}(b_m)y'_{n+1}(b_{n+1})\right] \\ & + \frac{H_4^1(E)}{2H_0^0(E)W\{y_{n+1}, z_{n+1}\}}\left[-z_{n+1}(b_{n+1})y'_{n+1}(b_m) + z'_{n+1}(b_m)y_{n+1}(b_{n+1})\right] \end{aligned} \tag{27}$$

where $y_{n+1}(x)$ and $z_{n+1}(x)$ in Equation (27) are the wave functions of the potential coupled to the arbitrary N potentials.

Since Equations (4) and (5) of the transcendental energy equation are similar, and Equations (6) and (7) of the group velocity and effective mass can also be obtained from the transcendental energy equation, it is reasonable to assume that these physical parameters can be generalized to more potentials and no longer only to one potential or two potentials coupled to a known potential. For the same reason, the following theorem and corollaries are proposed, whose detailed mathematical proof is presented in the Supplementary Materials.

5. Conclusions

Transcendental energy equations were solved for different periodic potentials that have solutions, such as the rectangular-like potential of negative intensity or in special functions such as linear-like potentials, which can be satisfactorily simulated numerically. Thus, it was possible to numerically calculate the behaviors of the group velocity and effective mass deduced from the modified transcendental energy equation. It was found that when the rectangular-like potential of positive intensity and the potential of negative intensity were coupled, the group velocity changed in its orientation at different heights and widths for both positive and negative rectangle intensities. This was reflected in the energy $H_0(E)$ function, which is the function that models the behavior of the group velocity. Table 1 shows some of the cases in which this orientation change occurred. From the numerical simulations carried out on the linear potentials, it was observed that the negative slope of the linear-like potential decayed faster than that found for the positive one. This is verified in Tables 2 and 3, both in the group velocity and in the effective mass for values of $b > a$ and $a < b$. These results led us to conclude that the width of the rectangle determines the decay as a function of the height of the linear-like potential,

governing both the maximum of the group velocity and the discontinuity energy of the effective mass. A significant contribution of this work was the development of the analytical generalization for N-coupled potentials to a rectangular-like potential as well as to a zero-like potential, whose corresponding equations are very important for the study of periodic potentials in solid state physics. These findings allow the calculation of equations for the generalization of an N-arbitrary potential connected to a potential $V(x)$ with special functions as a solution. These equations, however, cannot be expressed in the same form as Equations (23) and (24), which depend on hyperbolic and trigonometric functions, which are their linearly independent solutions. In addition, a 4×3 matrix was proposed, which is useful to achieve the generalization of N-coupled potentials together with an arbitrary potential. The Supplementary Materials provide the detailed proof of the novel theorem and its corollaries. The advantages of this study lie in the use of generalized equations, whereas the weaknesses of its method arise from the computing complexity associated with calculating additional potentials connected to a known potential.

Supplementary Materials: The following supporting information can be downloaded at https://www.mdpi.com/article/10.3390/app14103987/s1. Section S1: Left: Graphical scheme of the quantum potential representing the Kronig–Penney model and its corresponding parameters. Right: Energy curve graph for a rectangular-like potential; Section S2: Periodic potential of two potentials $V = V(x)$ and a rectangular-like potential; Section S3: The transcendental energy equation; Section S4: The group velocity; Section S5: The effective mass; Section S6: Generalization for N-coupled potentials to a known potential; Section S7: Generalization for N-coupled potentials together with another arbitrary potential; Section S8: Proof of the value of the determinant $H_0^0(E)$; Figure S1: Schemes of quantum potentials used in this work. The dark blue lines represent the Kronig–Penney potential. The magenta lines are due to the rectangular-like potential of negative intensity. The red and green lines represent the linear-like potentials, while the light blue and yellow lines are the triangular-like potentials; Figure S2: Numerical simulation of the transcendental energy equation for the periodic triangular-like potential ▲ together with the rectangular-like potential at different values of w. The height of the rectangle is $w_0 = 100$. The black solid lines correspond to the rectangular-like potential that simulates the Kroning–Penney model; Figure S3: Numerical simulation of the transcendental energy equation for the periodic triangular-like potential ▼ together with the rectangular-like potential at different values of w. The height of the rectangle is $w_0 = 100$. The black solid lines correspond to the rectangular-like potential that simulates the Kroning–Penney model; Figure S4: Numerical simulation of the energy $H_0(E)$ function for 30 energy values and for heights of 10, 25, 100, and 125 as indicated in the figure. The colors represent the simulated heights used in Figure 5.

Author Contributions: Conceptualization, F.M.-V. and J.A.R.-G.; methodology, F.M.-V. and J.A.R.-G.; software, F.M.-V.; validation, F.M.-V., E.V.M.-C., E.C.P. and J.A.R.-G.; formal analysis, F.M.-V., E.V.M.-C., E.C.P. and J.A.R.-G.; investigation, F.M.-V., E.V.M.-C., E.C.P. and J.A.R.-G.; resources, F.M.-V. and J.A.R.-G.; data curation, F.M.-V. and J.A.R.-G.; writing—original draft preparation, F.M.-V., E.C.P. and J.A.R.-G.; writing—review and editing, F.M.-V., E.V.M.-C., E.C.P. and J.A.R.-G.; visualization, F.M.-V. and J.A.R.-G.; supervision, F.M.-V., E.V.M.-C. and J.A.R.-G.; project administration, E.V.M.-C. and J.A.R.-G.; funding acquisition, E.V.M.-C. and J.A.R.-G. All authors have read and agreed to the published version of the manuscript.

Funding: We thank the "Programa de Subvención Financiera a Publicaciones de Investigadores UNMSM en Revistas Indizadas de Alto Impacto 2024" and Vicerrectorado de Investigación y Posgrado (VRIP) de la Universidad Nacional Mayor de San Marcos (UNMSM), Peru, for financially supporting this work. The APC was funded by VRIP-UNMSM.

Data Availability Statement: The raw data supporting the conclusions of this article will be made available by the authors on request.

Acknowledgments: Edson C. Passamani would also like to thank FAPES, TO-975/2022, and Conselho Nacional de Desenvolvimento Científico e Tecnológico (CNPq). Juan A. Ramos-Guivar also thanks PROCIENCIA, Project number 177-2020-FONDECYT.

Conflicts of Interest: The authors declare no conflicts of interest.

Appendix A

Theorem A1 (The Generalization Theorem for One-Dimensional Periodic Potentials). *This theorem states that if a periodic potential of period T is composed of arbitrary N-coupled potentials to a potential with known wave functions, then its transcendental equations of energy, group velocity, and effective mass are given by Equations (A1)–(A3).*

$$\cos(kT) = \Gamma(E) \tag{A1}$$

$$v_G = -\frac{T\sin(kT)}{\hbar}\left(\frac{d\Gamma(E)}{dE}\right)^{-1} \tag{A2}$$

$$m^* = -\hbar^2\frac{d\Gamma(E)}{dE}\left(T^2\cos(kT) + \frac{d^2\Gamma(E)}{dE^2}\hbar^2 v_G^2\right)^{-1} \tag{A3}$$

Proof of Theorem A1. The proof of this theorem is shown in Section S6 of the Supplementary Materials. □

Equations (A1)–(A3) represent the generalization of periodic potentials. These equations predict the shape of the group velocity and the discontinuity of the effective mass.

Appendix A.1

Corollary A1 (Corollary of Zero-Potential Generalization for One-Dimensional Periodic Potentials). *This corollary expresses the particular case in which the potential coupled to the arbitrary N potentials is zero. The equations corresponding to this approximation range from Equation (A4) to Equation (A9).*

$$\cos(kT) = \sin(\alpha a)\left[\frac{H_1^2(E)+\alpha^2H_4^2(E)}{2\alpha H_0^0(E)}\right] + \cos(\alpha a)\left[\frac{H_2^2(E)-H_4^1(E)}{2H_0^0(E)}\right] \tag{A4}$$

$$f_0(E) = \frac{H_1^2(E)+\alpha^2H_4^2(E)}{2\alpha H_0^0(E)} \tag{A5}$$

$$g_0(E) = \frac{H_2^2(E)-H_4^1(E)}{2H_0^0(E)} \tag{A6}$$

$$\Gamma_0(E) = \sin(\alpha a)\left[\frac{H_1^2(E)+\alpha^2H_4^2(E)}{2\alpha H_0^0(E)}\right] + \cos(\alpha a)\left[\frac{H_2^2(E)-H_4^1(E)}{2H_0^0(E)}\right] \tag{A7}$$

$$\frac{d\Gamma_0(E)}{dE} = \left(\frac{df_0(E)}{dE} - ag_0(E)\frac{d\alpha(E)}{dE}\right)\sin(\alpha(E)a) + \left(af_0(E)\frac{d\alpha(E)}{dE} + \frac{dg_0(E)}{dE}\right)\cos(\alpha(E)a) \tag{A8}$$

$$\begin{aligned}\frac{d^2\Gamma_0(E)}{dE^2} = &\left[\frac{d^2f_0(E)}{dE^2} - a^2f_0(E)\left(\frac{d\alpha(E)}{dE}\right)^2\right]\sin(\alpha(E)a) - \left[ag_0(E)\frac{d^2\alpha(E)}{dE^2} + 2a\frac{dg_0(E)}{dE}\frac{d\alpha(E)}{dE}\right]\sin(\alpha(E)a)\\ &+ \left[af_0(E)\frac{d^2\alpha(E)}{dE^2} + 2a\frac{df_0(E)}{dE}\frac{d\alpha(E)}{dE}\right]\cos(\alpha(E)a) + \left[\frac{d^2g_0(E)}{dE^2} + a^2g_0(E)\left(\frac{d\alpha(E)}{dE}\right)^2\right]\cos(\alpha(E)a)\end{aligned} \tag{A9}$$

Proof of Corollary A1. The proof of this corollary is shown in Section S7 of the Supplementary Materials. □

The energy functions $f_0(E)$ and $g_0(E)$ are generalized energy functions, which help to simplify the calculation of the group velocity and effective mass at the generalized zero potential.

Appendix A.2

Corollary A2 (Corollary of Rectangular Potential Generalization for One-Dimensional Periodic Potentials). *This corollary expresses the particular case in which the potential coupled to*

the arbitrary N potentials is rectangular. The equations corresponding to this approximation range from Equation (A10) to Equation (A15).

$$\cos(kT) = \sinh(\beta a)\left[\frac{H_1^2(E) - \beta^2 H_4^2(E)}{2\beta H_0^0(E)}\right] + \cosh(\beta a)\left[\frac{H_2^2(E) - H_4^1(E)}{2H_0^0(E)}\right] \tag{A10}$$

$$f_r(E) = \frac{H_1^2(E) - \beta^2 H_4^2(E)}{2\beta H_0^0(E)} \tag{A11}$$

$$g_r(E) = \frac{H_2^2(E) - H_4^1(E)}{2H_0^0(E)} \tag{A12}$$

$$\Gamma_r(E) = \sinh(\beta a)\left[\frac{H_1^2(E) - \beta^2 H_4^2(E)}{2\beta H_0^0(E)}\right] + \cosh(\beta a)\left[\frac{H_2^2(E) - H_4^1(E)}{2H_0^0(E)}\right] \tag{A13}$$

$$\frac{d\Gamma_r(E)}{dE} = \left(\frac{df_r(E)}{dE} + ag_r(E)\frac{d\beta(E)}{dE}\right)\sinh(\beta(E)a) + \left(\frac{dg_r(E)}{dE} + af_r(E)\frac{d\beta(E)}{dE}\right)\cosh(\beta(E)a) \tag{A14}$$

$$\begin{aligned}\frac{d^2\Gamma_r(E)}{dE^2} = &\left[ag_r(E)\frac{d^2\beta(E)}{dE^2} + 2a\frac{dg_r(E)}{dE}\frac{d\beta(E)}{dE}\right]\sinh(\beta(E)a) + \left[\frac{d^2f_r(E)}{dE^2} + a^2f_r(E)\left(\frac{d\beta(E)}{dE}\right)^2\right]\sinh(\beta(E)a)\\ &+ \left[af_r(E)\frac{d^2\beta(E)}{dE^2} + 2a\frac{df_r(E)}{dE}\frac{d\beta(E)}{dE}\right]\cosh(\beta(E)a) + \left[\frac{d^2g_r(E)}{dE^2} + a^2g_r(E)\left(\frac{d\beta(E)}{dE}\right)^2\right]\cosh(\beta(E)a)\end{aligned} \tag{A15}$$

Proof of Corollary A2. The proof of this corollary is shown in Section S7 of the Supplementary Materials. □

The energy functions $f_r(E)$ and $g_r(E)$ are generalized energy functions, which simplify the calculation of the group velocity and effective mass at the generalized rectangular potential.

Appendix A.3

Corollary A3 (Corollary of Group Velocity and Effective Mass in One-Dimensional Periodic Potentials). *This corollary states that the group velocity and effective mass of any periodic potential with a period T, composed of arbitrary N-coupled potentials to a potential with known wave functions, will then have an extreme value for the group velocity and a discontinuity point for the effective mass. These values can be computed using Equation (A16).*

$$0 = \frac{d^2\Gamma(E)}{dE^2} + \frac{1}{\sin(kT)\tan(kT)}\left(\frac{d\Gamma(E)}{dE}\right)^2 \tag{A16}$$

Proof of Corollary A3. The proof of this corollary is shown in Section S6 of the Supplementary Materials. □

The group velocity can reach a maximum or a minimum as a function of the energy band, as evidenced by the group velocity in Ref. [30]. Solving Equation (A16) provides the value of the wavenumber at which the extreme of the group velocity is obtained. Graphically speaking, the value of the wavenumber at which the discontinuity occurs is, interestingly, the same as that at which the extreme value of the group velocity is obtained. This is important because it allows the relation of the most important values of group velocity and effective mass to a single wavenumber value.

Appendix A.4

Corollary A4 (Corollary Approximation for the Dirac-Delta Potential in One-Dimensional Periodic Potentials). *This corollary states that if, in Corollary 1, the N potentials have the peculiarity that the global minima are at the extremes and the global maximum is*

located at the midpoint, then the Dirac-delta periodic potential can be approximated by the following limits of Equations (A17) and (A18).

$$\lim_{(b,w)\to(0,\infty)}(\alpha f_0(E)) = \lim_{(b,w)\to(0,\infty)}\left(\frac{H_1^2(E)+\alpha^2 H_4^2(E)}{2H_0^0(E)}\right) = F_d(b,w) \tag{A17}$$

$$\lim_{(b,w)\to(0,\infty)}(g_0(E)) = \lim_{(b,w)\to(0,\infty)}\left(\frac{H_2^2(E)-H_4^1(E)}{2H_0^0(E)}\right) = 1 \tag{A18}$$

Proof of Corollary A4. The proof of this corollary is shown in Section S7 of the Supplementary Materials. □

These limits of Equations (A17) and (A18) also represent a generalization to obtain the Dirac-delta periodic potential, as has been done in Ref. [30], but without making use of this generalization for arbitrary N potentials.

Appendix A.5

Corollary A5 (Corollary Approximation for the Kronig–Penney Potential in One-Dimensional Periodic Potentials). *This corollary states that if, in Corollary 2, the N potentials have the peculiarity that the global minima are found throughout the domain, then the periodic Kronig–Penney potential can be approximated by the following limits of Equations (A19) and (A20).*

$$\lim_{w\to 0}(f_r) = \lim_{w\to 0}\left(\frac{H_1^2(E)-\beta^2 H_4^2(E)}{2\beta H_0^0(E)}\right) = F_{kp}(b,w,E) \tag{A19}$$

$$\lim_{w\to 0}(g_r) = \lim_{w\to 0}\left(\frac{H_2^2(E)-H_4^1(E)}{2H_0^0(E)}\right) = G_{kp}(b,w,E) \tag{A20}$$

Proof of Corollary A5. The proof of this corollary is shown in Section S7 of the Supplementary Materials. □

The limits of Equations (A19) and (A20) also represent a generalization to obtain the periodic Kronig–Penney potential.

Appendix A.6

Corollary A6 (Schrödinger's Wronskian Corollary). *This corollary states that the determinant H_0^0 is proportional to the product of the Wronskians of the wave functions of the N potentials and is given by Equation (A21).*

$$H_0^0(E) = W\{y_1(x), z_1(x)\}\cdot\prod_{k=2}^{N}\left[(-1)^N\cdot W\{y_k(x), z_k(x)\}\right] \tag{A21}$$

Proof of Corollary A6. The proof of this corollary is shown in Section S8 of the Supplementary Materials. □

The value of the determinant $H_0^0(E)$ has been deduced using Wronskians, both for particular cases and as was done in Ref. [30]. This result was obtained by means of Abel's identity and by mathematical induction. It is also important because it is the only determinant for which a result was obtained properly.

Appendix B

To demonstrate that the theorem and corollaries are correct, Figure A1 shows graphically the fundamental diagram of the periodic potentials, in which the transcendental equations of energy, group velocity, and effective mass are shown for the rectangular-like potential of negative intensity.

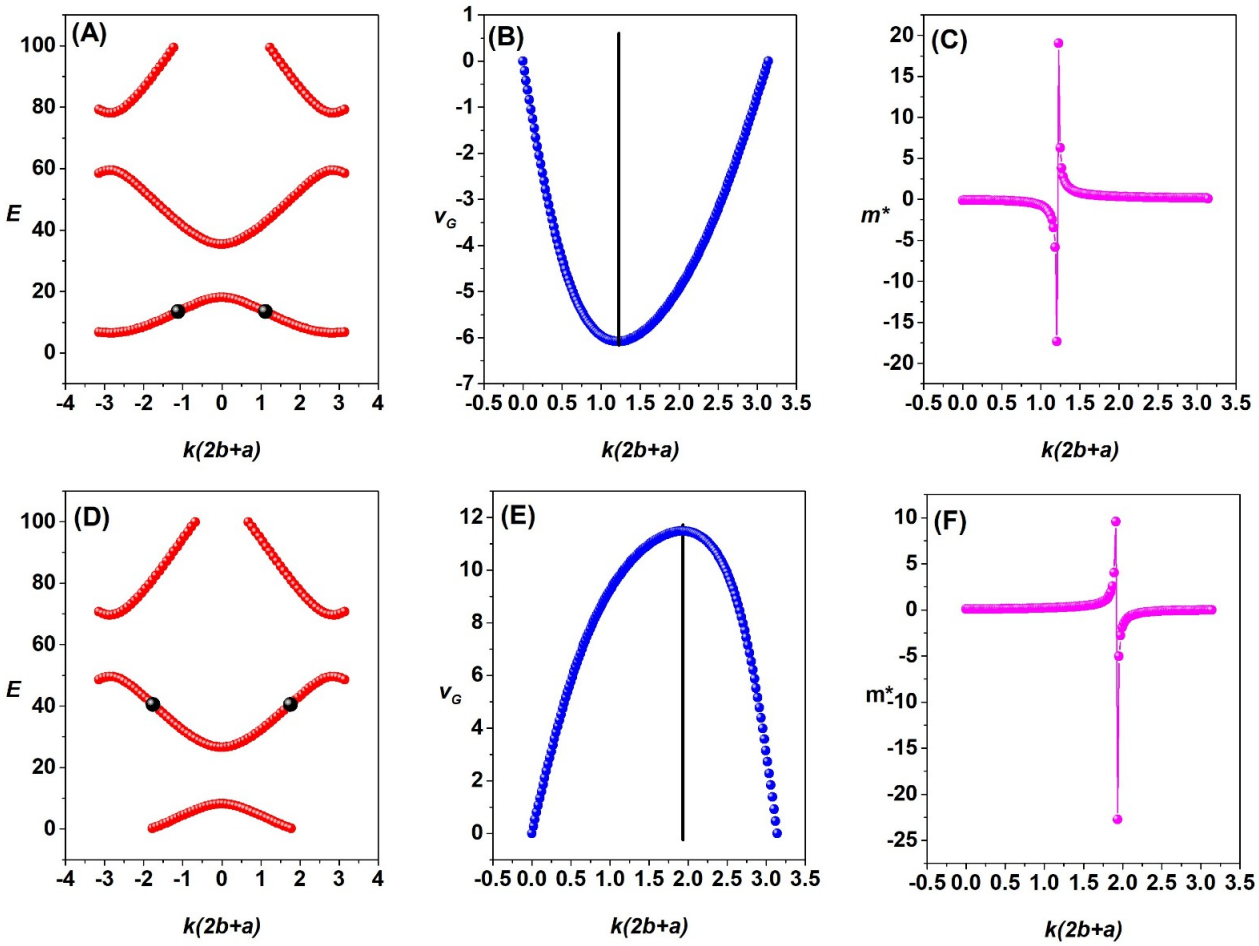

Figure A1. Numerical simulation with the values of $w_0 = 100$, $a = 1/10$, $b = 1/2$ for the transcendental energy equation, group velocity, and effective mass for the rectangular-like potential of negative intensity. The data were obtained for 150 energy values. (**A**–**C**) for height $w = 15$. (**D**–**F**) for height $w = 25$. The black dots and vertical black lines in (**A**,**D**) and (**B**,**E**) represent the value of k at which the extreme value of v_G and the discontinuity of m^* are reached.

The theory of odd and even functions predicts the negative part of the group velocity and the effective mass of the periodic potential. Since the energy is an even function, the group velocity is odd, and the effective mass is even. In addition, Figure A1 demonstrates that the intensity of the potential has an influence on the orientation of the group velocity, a notable difference from the potentials studied in Ref. [30]. Table A1 shows the kT-values that corroborate what was proposed in Corollary 3.

Table A1. Proof of Corollary 3 in the rectangular-like potential of negative intensity.

Group Velocity	w_0	a	b	kT	v_G
$w = 15$	100	1/10	1/2	1.23	−6.08
$w = 25$	100	1/10	1/2	1.93	11.5
Effective Mass	w_0	a	b	kT	E
$w = 15$	100	1/10	1/2	1.22	13.5
$w = 25$	100	1/10	1/2	1.92	40.5

Parameters of the periodic potentials diagram in Figure A1.

The results in Table A1 clearly demonstrate that the value of k at which the extreme value of the group velocity is reached is the same value of k at which the effective mass discontinuity exists. The corresponding error is $\Delta kT = 0.01$, while, in Tables 2 and 3, the errors are $\Delta kT = 0.05$. These results show that Corollary 3 is correct. In addition, the error value of ΔkT is mainly due to the energy values that have been used to perform the numerical simulation.

References

1. Singh, S. Manifestation of Quantum Mechanics and Particle Physics in the Macroscopic World. *J. Stud. Res.* **2022**, *11*, 1–5. [CrossRef]
2. Blount, E.I. Formalisms of band theory. *Solid State Phys.* **1962**, *13*, 305–373. [CrossRef]
3. Vidal, V.E.B. Gas de Bosones en Una Serie Finita de Capas Delgadas Penetrables. Bachelor's Thesis, Universidad Nacional Autónoma de México, Mexico City, Mexico, 2012.
4. Vargas, J.H. Método Generalizado de la Matriz de Transferencia (Mgmt); Método de las Funciones de Green de Superficie (Mfgs), Relaciones y Aplicaciones en Sistemas Semiconductores Periódicos. Master's Thesis, Universidad Nacional de Colombia, Bogota, Colombia, 2013.
5. Fernández, F.M. Dimensionless equations in non-relativistic quantum mechanics. *arXiv* **2020**, arXiv:2005.05377.
6. Mommadi, O.; El Moussaouy, A.; El Hadi, M.; Chnafi, M.; Meziani, Y.M.; Duque, C.A. Stark shift and exciton binding energy in parabolic quantum dots: Hydrostatic pressure, temperature, and electric field effects. *Philos. Mag.* **2021**, *101*, 753–775. [CrossRef]
7. Robinett, R.W. The Stark effect in linear potentials. *Eur. J. Phys.* **2009**, *31*, 1. [CrossRef]
8. Keebaugh, C.; Marshman, E.; Singh, C. Improving student understanding of corrections to the energy spectrum of the hydrogen atom for the Zeeman effect. *Phys. Rev. Phys. Educ. Res.* **2019**, *15*, 010113. [CrossRef]
9. Corona, G.P. Localización y Transporte en Medios Aleatorios en Una y Dos Dimensiones. Master's Thesis, Universidad Michoacana de San Nicolás de Hidalgo, Morelia, Mexico, 2017.
10. Le Vot, F.; Meléndez, J.J.; Yuste, S.B. Numerical matrix method for quantum periodic potentials. *Am. J. Phys.* **2016**, *84*, 426–433. [CrossRef]
11. Pavelich, R.L.; Marsiglio, F. The Kronig-Penney model extended to arbitrary potentials via numerical matrix mechanics. *Am. J. Phys.* **2015**, *83*, 773–781. [CrossRef]
12. Grosso, G.; Parravicini, G.P. *Solid State Physics*; Academic Press: London, UK, 2013.
13. Escudero, F.J. Conductores, aislantes y semiconductores. *DYNA* **1967**, *42*, 113–140. Available online: https://www.revistadyna.com/busqueda/conductores-aislantes-y-semiconductores (accessed on 31 January 2024).
14. Ashcroft, N.W.; Mermin, N.D. *Solid State Physics*; Cengage Learning: Boston, MA, USA, 1976.
15. Moore, E.A.; Smart, L.E. Optical properties of solids. In *Solid State Chemistry*; CRC Press: Boca Raton, FL, USA, 2020; pp. 283–314.
16. Merzbacher, E. The early history of quantum tunneling. *Phys. Today* **2002**, *55*, 44–50. [CrossRef]
17. Gupta, R.; Singhal, T.; Verma, D. Quantum mechanical reflection and transmission coefficients for a particle through a one-dimensional vertical step potential. *Int. J. Innov. Technol. Explor. Eng.* **2019**, *8*, 2882–2886. [CrossRef]
18. de Oliveira, E.C.; Vaz, J. Tunneling in fractional quantum mechanics. *J. Phys. A Math. Theor.* **2011**, *44*, 185303. [CrossRef]
19. Heim, D.M.; Schleich, W.P.; Alsing, P.M.; Dahl, J.P.; Varro, S. Tunneling of an energy eigenstate through a parabolic barrier viewed from Wigner phase space. *Phys. Lett. A* **2013**, *377*, 1822–1825. [CrossRef]
20. Elabsy, A.; Attia, M. Quasi-resonant tunneling states in triangular double-barrier nanostructures. *Res. Sq.* **2023**. [CrossRef]
21. Mendoza, J.A.; López, J.C.; Suárez, R.M. Análisis del comportamiento de un potencial lineal al solucionar la ecuación de Schrödinger. *BISTUA Rev. Fac. Cienc. Básicas* **2021**, *18*, 34–37.
22. Yuce, C. Quantum inverted harmonic potential. *Phys. Scr.* **2021**, *96*, 105006. [CrossRef]
23. Soto-Eguibar, F.; Moya-Cessa, H.M. Solution of the Schrödinger equation for a Linear potential using the extended Baker-Campbell-Hausdorff formula. *Appl. Math. Inf. Sci.* **2015**, *9*, 175. [CrossRef]
24. Gil, A.; Segura, J.; Temme, N.M. Fast and accurate computation of the Weber parabolic cylinder function W (a, x). *IMA J. Numer. Anal.* **2011**, *31*, 1194–1216. [CrossRef]

25. Abramowitz, M.; Stegun, I.A. *Handbook of Mathematical Functions: With Formulas, Graphs, and Mathematical Tables*; Dover Publications: Mineola, NY, USA, 1965.
26. Sun, G.H.; Chen, C.Y.; Taud, H.; Yáñez-Márquez, C.; Dong, S.H. Exact solutions of the 1D Schrödinger equation with the Mathieu potential. *Phys. Lett. A* **2020**, *384*, 126480. [CrossRef]
27. Dong, S.H.; Dong, S.; Dong, Q.; Sun, G.H.; Femmam, S. Exact solutions of the Razavy cosine type potential. *Adv. High Energy Phys.* **2018**, *2018*, 5824271. [CrossRef]
28. Chen, C.Y.; Lu, F.L.; Sun, G.H.; Wang, X.H.; You, Y.; Sun, D.S.; Dong, S.H. Exact solution of rigid planar rotor in external electric field. *Results Phys.* **2022**, *34*, 105330. [CrossRef]
29. Chen, C.Y.; Wang, X.H.; You, Y.; Sun, D.S.; Lu, F.L.; Dong, S.H. Exact solutions to the angular Teukolsky equation with $s \neq 0$. *Commun. Theor. Phys.* **2022**, *74*, 115001. [CrossRef]
30. Mendoza-Villa, F.; Ramos-Guivar, J.A.; Espinoza-Bernardo, R.M. Generalized One-Dimensional Periodic Potential Wells Tending to the Dirac Delta Potential. *Physics* **2024**, *6*, 75–93. [CrossRef]
31. Carver, T.R. Mathieu's functions and electrons in a periodic lattice. *Am. J. Phys.* **1971**, *39*, 1225–1230. [CrossRef]
32. Yang, Z. Non-perturbative Breakdown of Bloch's Theorem and Hermitian Skin Effects. *arXiv* **2020**, arXiv:2012.03333.
33. Alvarez, L. Introduction of the concepts of hole and effective mass using an alternative to the Ek diagram. *Rev. Mex. Fís.* **2013**, *59*, 128–132.
34. Náraigh, L.Ó.; O'Kiely, D. Homogenization theory for periodic potentials in the Schrödinger equation. *Eur. J. Phys.* **2012**, *34*, 19. [CrossRef]
35. Bloch, I. Ultracold quantum gases in optical lattices. *Nat. Phys.* **2005**, *1*, 23–30. [CrossRef]
36. Izquierdo, E.A. Funciones de Green Aplicadas a la Solución de Problemas de Contorno Basados en la Ecuacion Diferencial de Airy. Bachelor's Thesis, Universidad de Narino, Pasto, Colombia, 2018.
37. Gil, A.; Segura, J.; Temme, N.M. Numerical Evaluation of Airy-Type Integrals Arising in Uniform Asymptotic Analysis. *J. Comput. Appl. Math.* **2020**, *371*, 112717. [CrossRef]